FIRST BREAKS - AUTOMATIC PICKINGS OF P- AND S- ONSETS IN SEISMIC RECORDS

Eystein S. Husebye[1]) and Yu. V. Fedorenko[2])

1) Institute Solid Earth Physics, University of Bergen, Norway
2) Institute North Ecology Problem, Kola Science Center RAS, Russia

Sponsored by the Defense Treat Reduction Agency
Department of Defense, U.S.A.

Grant DSWA0I-98-C-0159

ABSTRACT

With an ever increasing number of seismic stations deployed worldwide partly under the IMS/CTBTO/UN umbrella there is an obvious need to automate seismic phase pickings. The problem is naturally most acute for local event records since they are most numerous and besides are most complex. We have previously addressed this problem in terms of easily picking maxima in envelope transformed records (Husebye et al., BSSA, 1999) which proved efficient for picking Lg-phases. As a needed improvement to this analysis tool, we have developed, validated and tested a versatile processing scheme for picking with confidence P- and S- onsets in local records. Out of 300 events analyzed accurate phase arrival times were picked for 90% of these recordings. Essential ingredients in the processing scheme were i) prewhitening, ii) wavelet transform, iii) polarization filter, iv) envelope transform and v) model function fitting by a simulated annealing method for picking first breaks in an optimal manner in approximately noise free envelope records. Automatic signal analysis implies extraction of a failure diagnostic for activating manual record inspections when need be. Ours are tied to relative energy distributions in the records and despite its simplicity work well. Our P- and S-pickings were converted to epicenter distances using a simple crustal model and then compared to corresponding estimates derived from the local bulletins. A qualitative comparison to analyst (bulletin) results were obtained for 2 separate a priori known explosion sites; our epicenter exhibited less scattering than those of the analyst. Out of the 10 % events classed as picking failures, a few were due to corrupted records while others were too messy even for manual analysis. However, the majority was due to processing errors and the reason being mainly that the function fitting algorithm picked secondary ripples on the dominant S/Lg-envelope. In view of the success in picking P- and S- arrival times for local events we are now adapting concept for picking in an automatical manner also teleseismic P-arrival times.

Key Words: Phase pickings, wavelet transform, polarization, envelope, function fitting, simulated annealing.

OBJECTIVE

The objective of this research is to facilitate to the extent possible automatic pickings of P- and S-phases in seismic records. This remains an outstanding problem in observational seismology and particularly in the context of CTBTO/IMS global seismic monitoring since such tasks still are somewhat manual. The very efficiency of the IMS global monitoring system requires that feature extractions in terms of phase arrivals, signal amplitudes and so forth are automated to the extent of minimum analyst interference. The major element in the research strategy chosen, was to tie analysis to slowly varying signal envelopes and not to the fast varying signals typical of the original waveform records. To achieve this objective, essential ingredients in seismic record analysis are i) prewhitening, ii) wavelet transform, iii) polarization, iv) envelope transform and v) function fitting by a simulated annealing method for picking first breaks in approximately noise free envelope records. The initial research stage our efforts are focused on P- and S-picking in local records which are more complex that those for teleseismic distances.

RESEARCH ACCOMPLISHED

A persistent and outstanding problem in observational seismology is that of confidentially picking P- and S-phases in local event records. These records are not only complex in view of the "sensitivity" of high frequency waves to small scale crustal heterogeneties but also because it is not always clear which phase arrivals are actually present in the records. Ambient noise often tends to mask the first cycle of the P- onset so picking errors are non-Gaussian. Such problems are more adverse for S- signals which arrive in the tail of the P- coda and besides have a more complex propagation path including phase conversions and scattering contributions (Hestholm et al., 1993; Sato and Fehler, 1998). The aim of this study was to develop a more robust and reliable phase picking scheme and in this regard discard the conventional waveform phase picking approach. Instead we focused on signal envelope processing schemes since both P- and S- envelope appear far more stable and recurrent than their respective original waveform segments (Husebye et al., 1998). An additional advantage with signal envelopes is that phase arrival times are tied to the envelope peak where SNR is good in comparison to the P- onset in the original waveform segment. Other approaches are to stack envelope transferred records from a network of stations thus mimicking seismic array beamfoming (Ryzhikov et al., 1997, Kushnir et al., 1999). Most of these processing schemes are often simplistic and seems to ignore a basic feature of envelopes which may be visualized via WKBJ synthetics for laterally homogeneous media. The characteristic features here are sharp P- and S- onsets and after being transformed into envelopes look like pulses of short duration. Another characteristic feature is exponential P- and S- coda decays that are typical of real seismograms (Sato and Fehler, 1998). Taking this into account we may expect that the shape of an envelope of real waveform will be close to that shown in Fig. 1.

Data used in analysis stem from segmented event recordings in the 30-300 km range from the 3-component (3C) station Hoyanger (HYA) in western Norway (Fig. 2). The original records (example in Fig. 3a) are our raw material and is not useful for further analysis unless refined. With refinement is meant suppressing ambient and signal generated noise and then envelope phase shaping as implied in Fig. 1. To achieve this we introduced a waveform processing sequence comprising 4 steps; i) prewhitening, ii) wavelet transform, iii) polarization filtering and iv) envelope smoothing and v) functional fitting. The various processing techniques used, are detailed below and besides illustrated in Fig. 3. Our research accomplishments are tied to analysis of 300 local events recorded at a station on the west coast of Norway. The epicenter distance range is 25 - 250 km ensuring the full complexity of local event recordings and thus taken intuitively to be representative of local events anywhere. Below, analysis procedures are described in some detail and starting with 'record prewhitening' as our first step here.

Raw traces and prewhitening

The prewhitening has a dual purpose of removing low-frequency part of ambient noise and producing an approximate white noise spectrum as desired for the subsequent wavelet transform. With basis in many spectral studies we may use a simple linear noise spectrum representation that is inverse proportional to frequency ω. Ambient noise exhibit at least in coastal areas strong seasonal variations in levels but not in form for $f >$ I Hz so the "inverse ω" shape provides a robust and versatile spectrum representation. Using

this noise feature we can easily transform initial seismic traces into traces with "white" seismic noise simply by differentiation. The fastest numerical procedure is to apply FFT to the initial traces, multiply resulting spectra by $i\omega$ $\left(i = \sqrt{-1}\right)$ in frequency domain and then transform it back to time domain. Alternatively, we may use the so-called IIR high-pass filter of order 1 with cut-off frequency close to Nyquist frequency for prewhitening. The latter is more flexible because we can apply sequentially different filters to suppress "hump" in the noise spectra often observed for $1 < f < 2$ Hz. Anyway, raw traces are shown in Fig. 3a while those obtained after prewhitening are shown in Fig. 3b. The striking gain in SNR was not unexpected as the local noise is dominated by surf on the nearby coast. By bandpass filtering or optimal variants hereof (Kushnir at al., 1999) better noise suppression may be obtained. However, "gain" depends on both noise and signal spectra which makes bandpass filtering not suitable for our purpose.

Wavelet transform.

Like the Fourier transform (FT), the wavelet transform (WT) is a linear operator on a data vector whose length usually is an integer power of 2, transforming it into a numerically different vector of the same length. In the wavelet domain basis functions $\psi(\tau, s; t)$ are somewhat complicated and have fanciful names like 'mother functions' and 'wavelets'. WT can be thought of as $X(\tau, s) = \int x(t)\, \psi_{\tau s})(t)dt$ where $\psi_{\tau s}(t) = (1/\sqrt{s}\,)\, \psi)[(t - \tau)/s]$. In the WT domain the axes are scale s or inverse frequency and τ which is time shift as the wavelet slides through the signal window. Physically this means that low scales which is the high frequency part of the signal has good time resolution while high scales are low frequencies with good frequency resolution. Hence, most of the usefulness of wavelet operation rests on the fact that $X(\tau, s)$ can be severely truncated (Press et al., 1992) thus removing weakly represented scattering and noise contributions. The choice and corresponding length of the wavelet function does not appear to be overly critical; after much experimenting with wavelets of the types Daubechies 4, 12 and 20, we settled for Daubechies 20 (Daubechies, 1988; Press et al., 1992). In practical seismogram analysis we expect that in the case of pure noise with approximately flat spectra after prewhitening the wavelet transform will also be flat so wavelet coefficients for different s and τ will possess similar amplitudes which may be removed without substantial distortion of the seismic signal.

To test this hypothesis and assess the truncation threshold level we computed empirical probability density function (p.d.f) of wavelet coefficients for pure noise samples. According to this p.d.f the truncation at threshold level of 20 must remove 99.9% of wavelet coefficients corresponding to noise. Testing of real data is illustrated in Fig. 3c; the noise preceding incoming P- and S- waves is not only reduced - it is literally wiped out. The P- and S- signals as such are not much distorted except that small "ripples" have been removed so more smooth signals and shorter codas appearances have been obtained.

Polarization filter

To enhance P and S onsets and to suppress various kinds of coda waves we applied polarization filtering. Following Christoffersson et al. (1988) and Jepsen and Kennet, (1990), we assume that seismic signal $s(t)$ $[{}^{s}N(t), {}^{s}E(t), {}^{s}D(t)]^{T}$ containing both P and S waves may be represented as

$$s(t) = [\sin\phi \cos\theta, \sin\phi \sin\theta, \cos\phi]^{T} s(t)$$

Here, $s(t)$ is the plane wave amplitude, θ - azimuth and ϕ apparent angle of incidence on the free surface. The relation between "true" and apparent incident angles are $\tan\phi = F \tan i$ where F is surface correction factor. The latter is given by $F = 2 \cos i \cos j / (1 - 2\sin^2 j)$ where i would be the actual angle to the vertical made by the normal to the plane wave front, and j is the true propagation angle for SV wave which is related to i via Snell's law. If the angle of incidence j is greater than the critical angle j_c, surface displacement for SV waves may be written as

$$s(t) = [i \sin\phi \cos\theta, i \sin\phi \sin\theta, \cos\theta]^{T} s(t)$$

This expression is also appropriate for higher and fundamental mode Rayleigh waves, but here ϕ = arctan e where |e| is the eccentricity of elliptical motion. We used Hilbert transform to make complex traces $\hat{s}_i$ from real traces s_i and to produce complex covariance matrix $C_{ij} = \hat{s}_i \hat{s}_j^*$ where i, j = 1, 2, 3 and an asterisk means "complex conjugate". The expression for polarization filtering P(t) used in this study is:

$$P(t) = \frac{(C_{13}^2 + C_{23}^2)(C_{11} + C_{22} + C_{33})}{(C_{11} + C_{22})\, C_{33} + \gamma} \qquad (1)$$

where γ is a small number to ensure numerical stability. As may be easily shown, P (t) has following properties: i) Re [P (t)] does not depend explicitly on ϕ and θ, ii) if the seismic signal is pure linearly polarized, Re [Prect(t)] =$|s(t)|^2$> 0, iii) if the seismic signal is pure elliptically polarized, Re[Pell(t)] = - s(t), ${}^{s}E(t)\ {}^{s}D(t)$ elements are uncorrelated, < Re[P (t)] > → 0,

These properties make the filter operator $P(t)$ useful for enhancing P and S arrivals as demonstrated in Fig. 3d. The imaginary part of $P(t)$ appears if and only if the seismic signal is a mixture of linearly and elliptically polarized components, which is always the case with ambient noise and coda waves present. For both pure linear and pure elliptical polarization Im[$P(t)$] = 0. The latter properties of the polarization filter operator (1) were of no use in our analysis. Important, our polarization filtering approach allows us to exclude time domain averaging in record analysis so the original sharp P- and S- onsets are retained which in turn are essential for improving (at least maintaining) phase picking accuracy.

Nonlinear smoothing.

Picking of P- and S- onsets directly from the polarization filter would obviously not be a good idea in view of the spiky and irregular appearances of the output records (Fig. 3d). To make phase picking more robust we apply nonlinear smoothing to the polarization filter output E(t_i) by the recursive formula:

$$E(t_i) = \begin{cases} E(t_i) & \text{if } E(t_i) > E(t_{i-1}) \\ E(t_{i-1}) \exp(-\lambda \Delta t), & \text{if } E(t_i) < E(t_{i-1}) \end{cases}$$

where i = 1, ..., N, N is number of samples in the polarization filter output, Δt sampling interval, in our case Δt = 0.02 s, $t_i = (i - 1)\,\Delta t + t_b$, t_b is UT of recording triggering, parameter λ controls the decay of resulting envelope. The choice of λ was a compromise between 2 extremes; if λ small a spiky record would produce boxlike envelopes while too large the polarization records would be retained without too much distortions. Our choice of λ = 0.05 produced envelope shapes like that shown in Fig. I and besides being sensitive enough to preserve a weak S-wave onset. Naturally this λ - decay is similar to that characterizing observational S-coda roll-off (Sato and Fehler, 1998). Anyway, at this processing step it may be instructive to compare the prototype in Fig. 1, original raw traces in Fig. 3a and the corresponding envelope variant in Fig. 3e; phase picking should be easier in the latter case.

Function fitting - phase fitting.

Due to the simplistic shape of the polarization envelope it may be tempting to read onset times manually but an automatic manner is naturally preferable. Our starting point here was the Fig. 1 envelope which

served as the prototype for the 'record processing end product' or last processing step. On analytical form the Fig. 1 functional representation is:

$$F_e(t) = \begin{cases} 0; & t \quad [t_0, t_1) \\ A_1(t - t_1), & t \quad [t_1, t_2) \\ h_1 \exp[\alpha_1 (t - t_2)], & t \quad [t_2, t_3) \\ A_2(t - t_3) + B_2, & t \quad [t_3, t_4) \\ h_3 \exp[\alpha_2 (t - t_4)], & t \quad [t_4, t_5) \end{cases}$$

Here $A_1 = h_1/(t_2 - t_1)$, $\alpha_1 = log(h_1/h_2)/(t_3 - t_2)$, $A_2 = (h_3 - h_2)/(t_4 - t_3)$,
$B_2 = (h_2 t_4 - h_3 t_3)/(t_4 - t_3)$, $\alpha_2 = log(h_3/h_4)/(t_5 - t_4)$ with the obvious constraints $t_1 < t_2 < t_3 < t_4 < t_5$, $h_4 < h_3$. Using this prototype we can formulate the problem of seismic phases fitting as finding the global minimum $\left[t_1^{min}, t_2^{min}, t_3^{min}, t_4^{min}, h_1^{min}, h_2^{min}, h_3^{min}, h_4^{min}\right]$ of the objective function:

$$\Phi(t_1, t_2, t_3, t_4, h_1, h_2, h_3, h_4) = \sum_{k=1}^{N} F_e((i-1) * \Delta t) - E_i)^2 \qquad (3)$$

Finding the global minimum is always a difficult problem. In our case we have tested almost all numerical quasi-Newton methods which failed apparently because of convergence towards local minima in (3). The method of simulated annealing in Press et al., (1992) proved adequate to find a global minimum for Φ (...) in eq. 3. A good initial guess is important for optimization problem. There are two possibilities to start the optimization process - either to estimate P-onset using the STA/LTA detector triggering time that is t_1^{min} or to find the maximum E_i and estimate t_2^{min} or t_4^{min}. Using maximum of envelope appears to be more robust than seeking for the P-onset but in the former case we must differentiate between t_2^{min} or t_4^{min} to know whether P-onset is larger than S. To resolve this problem we considered the following diagnostic:

$$D = \frac{S_r - S_l}{S_r + S_l}$$

with $S_l \sum_{1}^{i_{max}-1} E_i$, $S_l = \sum_{i_{max}}^{N} E_i$ where E_i is the smoothed polarization filter output and i_{max} being index for dominant envelope peak. For large S-phase (P weak) $D > 0.65$ implied failure while for P large (S weak) $D < 0.85$ implied failure. In other words, the above D-diagnostic prove reliable in 'triggering' analyst inspection of records and processing results.

Processing scheme summary.

The first 3 steps are straightforward while those of polarization envelopes and functional fitting proved rather cumbersome. The reason for this was our emphasis on robustness in processing without restoring to a multitude of alternative schemes in order to incorporate local seismogram oddities. Of course it would be feasible to modify scheme for picking teleseismic P-onsets including a search for depth phases like pP and sP - we are actively working on this now. Other application will be signal detection (no functional fitting) to use explosion envelopes as multidimensional source features for explosion site recognitions (Fedorenko et al., 1998, 1999).

Bulk analysis of local events.

The 303 events subjected to analysis occurred in 1996 - 1997 and their real distribution is shown in Fig. 2. The raw traces for the Hoyanger (HYA) station were extracted from segmented event files and then processed without human interferences in the manner described in the previous section. The measure used for testing performances was estimated epicenter distances derived by converting (t_S - t_P) times using a

simple crustal model. These distance estimates were in turn compared to those for HYA in the local bulletins as shown in Fig. 4. More than 63 % of the automatically processed events were within 10 km of those in the bulletin while the remaining ones differ in extreme by 90 km. The bulletin epicenter solutions are not error free not at least because the network configuration is much elongated in the N-S direction giving poorer E-W resolutions. Hence, a more objective performance test was to compare 'absolute' distances since we had at hand ground truth information from 2 explosion sites at Geiranger and Mongstad respectively (Fig.2; Fedorenko et al., 1999). Not too surprising our automated distance estimates exhibit lesser scattering than those in the bulletins (Fig. 4 caption). The small distance biases of ca 4-5 km seen here is of little interest since the crust is not entirely homogeneous. In Fig. 4 events with distance differences exceeding 20 km are of special interest - what went wrong? Close examinations of these outliers gave that 3 was caused by corrupted records, a few reflected large bulletin errors but most processing failures. The reason here was that the function fitting algorithm picked secondary ripples on the dominant envelope as an independent P- or S-phase so large distance errors ensued. For 7 events the fitting algorithm was not activated because *D*-diagnostic fell into the uncertain range $0.65 < D < 0.8$. In 4 of these cases the P-envelope was very weak (P-onsets correct!) while in the 3 other cases both us and the fitting algorithm were confused. The above results give that our new processing and phase picking scheme handle approximately 90 % of events analyzed in a most satisfactorily manner.

CONCLUSIONS AND FUTURE PLANS

Automating seismogram analysis has been a prime research topic for more than 3 decades but progresses have been moderate in contrast to interactive seismogram analysis. The main reasons for this appear to be the inherited complexities in local P- and S-wavefield recordings with signal correlations decreasing rapidly between stations being located even less than a kilometer apart. As demonstrated here, signal envelopes have a rather simplistic shape and as such can successfully be used for very accurate pickings of both P- and S-arrival times for 300 local events (Fig. 2 and 4). Our success rate of 90% for the event analyzed and with a performance matching or even better than that tied to manual analyst analysis. These results are indeed encouraging and the next step is joint analysis of all network recording stations in order to demonstrate that the ultimate goal of automated bulletin production perhaps is achievable. However, analyst inspections and event verifications are likely to be needed for the foreseeable future but he/she may be triggered into actions by specific acceptance criteria as also attempted by us. So far we have limited our research work to local events (most complex) but foresee few problems in extending analysis to teleseismic phases like P, pP and sP. Finally, any seismograph station represents a partly unique recording environment so our processing sequences and associated parameterizations albeit robust and flexible are not obviously transportable.

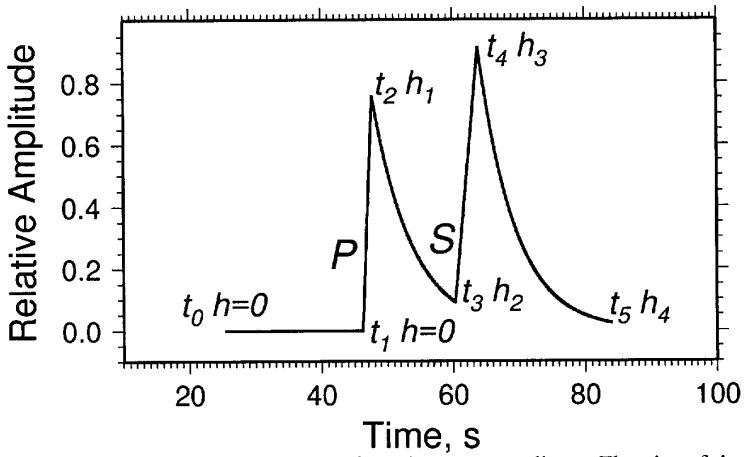

Fig. 1. Prototype $F_e(t)$ of envelope transform of local event recordings. The aim of the record processing sequences is to produce such envelopes. The h- and t- parameter mark extremes of the envelope prototype (definitions in eq. 2), and t_1 and t_3 would be equivalent to P- and S- phase arrival times. The actual picking of t_1 and t_3 is through functional fitting (simulated annealing) and is discussed in text.

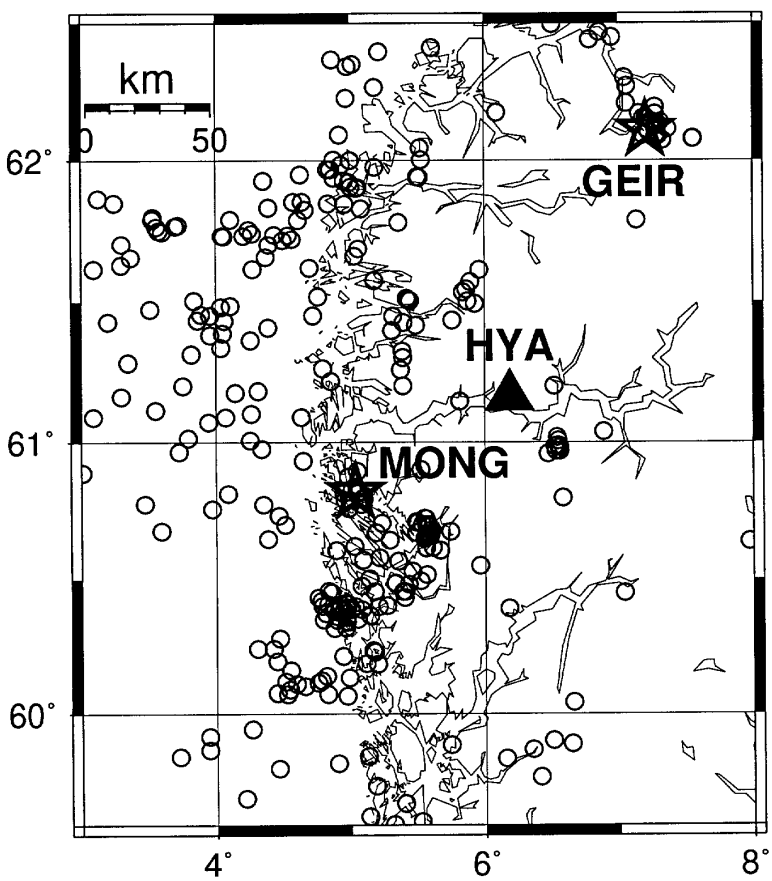

Fig. 2. Map showing the epicenters for all 300 events subjected to automatic P- and S-pickings. The 3-component station Hoyanger (HYA) is special marked and likewise the 2 explosion sites for which ground truth information were avaiable (GEIR=Geiranger; MONG=Mongstad).

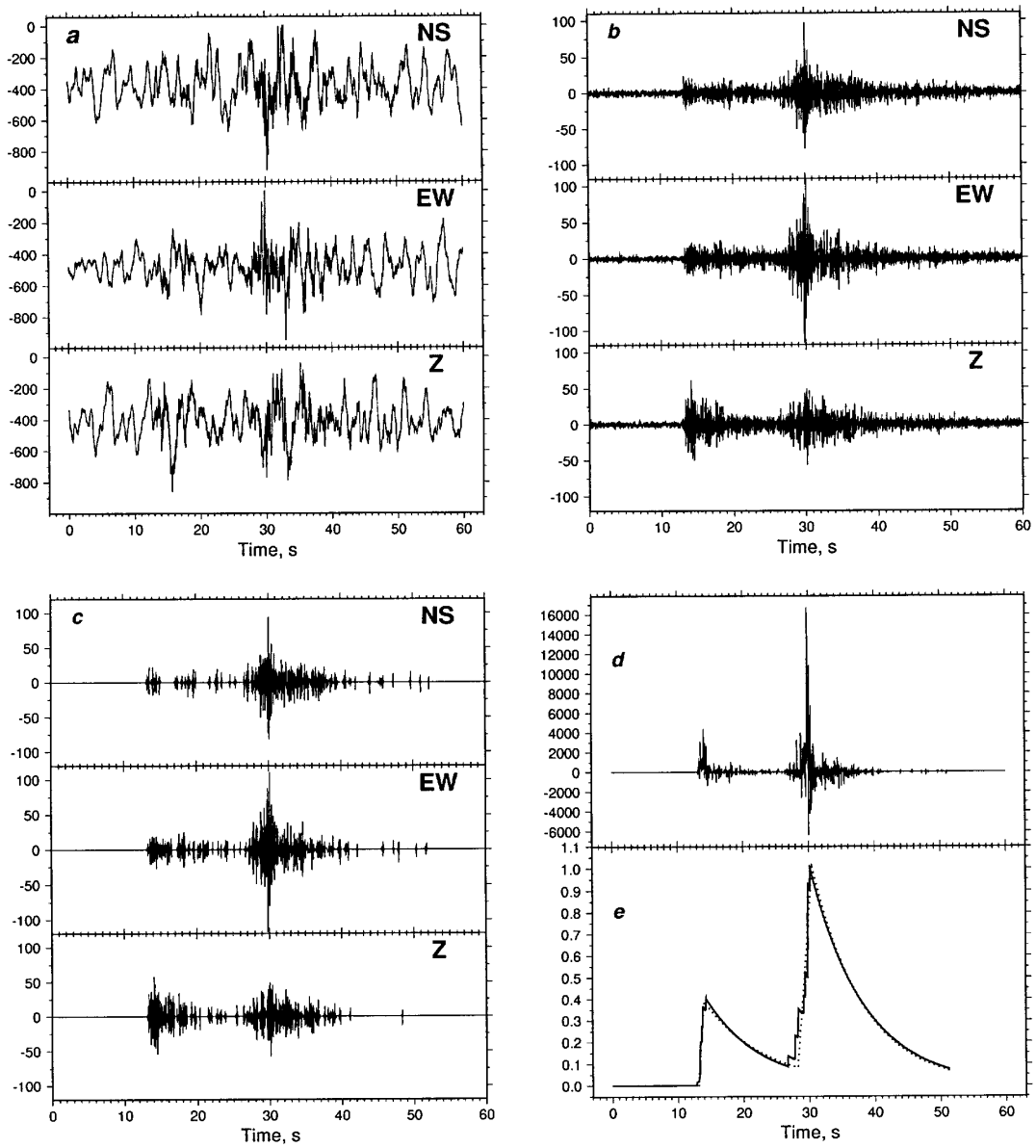

Fig. 3. Original waveform processing. Fig. 3a: Raw waveforms that is unfiltered Hoyanger (HYA) 3-component (3C) recording of an arbitrarily chosen event in our data base. Focal parameters are: Date 12/03/96, OT 14/09/46.0, 60.13 N 4.99 E, H = 0.0, ML = 1.5; Fig. 3b: Same event as in 3a but after prewhitening filtering; noise suppression is significant. Fig. 3c: Same event as in 3a but after wavelet transform operation; preceeding noise has been wiped out while the signal segments remain largely unscatched. However, the later parts of both the P- and S-coda, mainly attributed to multiscattering wavelets, are effeciently suppressed; Fig. 3d: Same event as in 3a but after polarization 'filtering', both P- and S-wave trains are cleaner implying contributions from out-of-plane reflections and refractions in the original waveforms; Fig. 3e: Same event as in 3a but after evelope transform and function fitting (dotted line); P- and S-phase pickings at 'start time' for the 2 envelopes as detailed in Fig. 1.

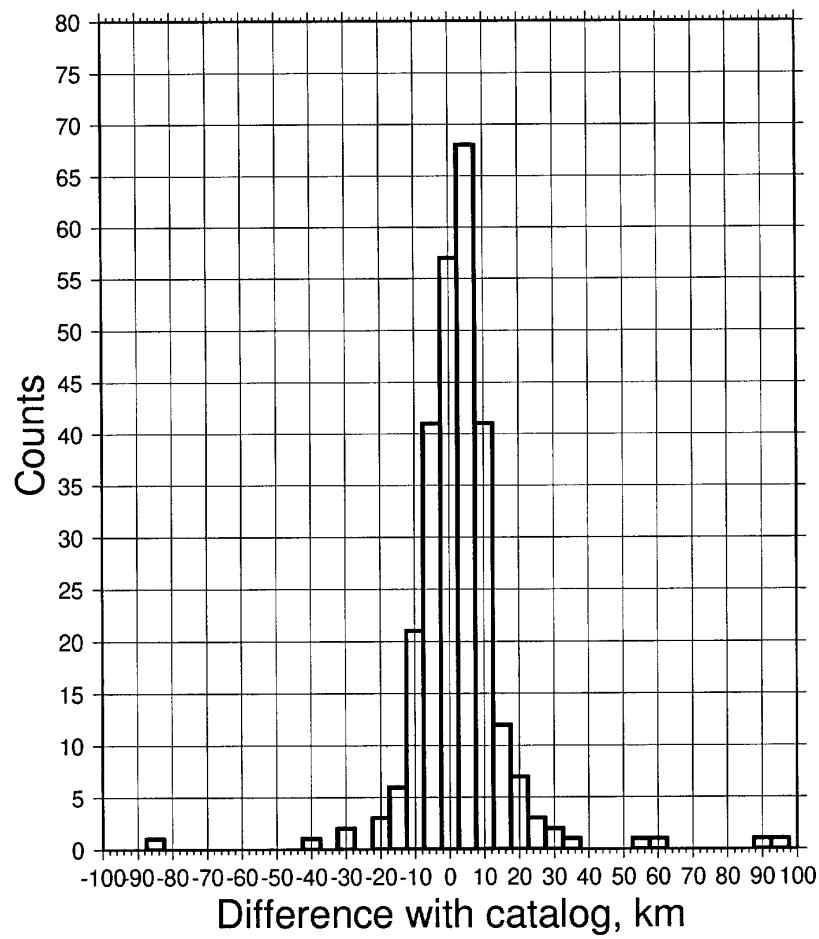

Fig. 4: Performance of the automatic phase picking algoritm for the 300 local events analyzed (Fig. 2). The $t_S - t_P$ differential times were converted to epicenter distances using a simple crustal model and then compared to Hoyanger epicenter distances as listed in the local bulletins. For the known explosion at sites Mongstad and Geiranger (Fig. 2) our distance estimates were more consistent than those in the bulletins that is within bounds of ± 2 km (ours) versus ± 4 km (bulletin) for a total of 20 explosions. Most of the outliers in the figure, differences exceeding 20 km, were caused by minor (10%) pecularities in the phase pickings as detailed in text.

REFERENCES

Christoffersson, A., E. S. Husebye and, S. F. Ingate, 1988. Wavefield decomposition using ML probabilities in single site 3-component records. Geophys. J. 93, 197-213.

Daubechies, I. 1988. Communications on Pure and Applied Mathematics, vol. 41, pp. 909-996.

Fedorenko, Yu. V, E. S. Husebye, B. Heincke and B. O. Ruud, 1998. Recognizing explosion sites without seismogram readings: neural network analysis of envelope-transformed multistation SP recordings 3-6 Hz. Geophys. J. Int. 133, F 1-F6.

Fedorenko, Yu. V, E. S. Husebye and B. O. Ruud, 1999. Explosion site recognition; neural net discriminator using three-component stations. Phys. Earth Planet. Int., June 1999 issue.

Hestholm, S. O., E. S. Husebye and B. O. Ruud, 1994. Seismic wave propagation in complex crust-upper mantle media using 2-D finite difference synthetics. Geoph. J. Int. 118, 643-670.

Husebye, E. S., B. O. Ruud, and A. M. Dainty, 1998. Fast, robust and reliable epicenter determinations: envelope processing of local network data. Bull. Seismol. Soc. Am. 88, 284-290.

Jebsen, D. C. and B. L. N. Kennett, 1990. Three-component analysis of regional seismograms. Bull. Seismol. Soc. Am., 80, 2032 - 2052.

Kushnir, A. F., E. V. Troitsky, , L. M. Haikin and A. M. Dainty, 1999. Study of statistical classification approach to discrimination between weak earthquakes and chemical explosions recorded by the Israel local seismic network. Phys. Earth Planet. Int., June 1999 issue.

Press, W. H., S. A. Teukolsky, W. T. Vetterling and B. P. Flannery, 1992. Numerical Recipes in C: The Art of Scientific Computing, Chap. 13, 2nd Edition, Cambridge University Press, MA, USA.

Ryzhikov, G.A., M. S. Biryulina and E. S. Husebye, 1997. A novel approach to Automatic Monitoring of Regional Events. IRIS Newslett. 15, 12 - 14.

Sato, H. and M. C. Fehler, 1998. Seismic Wave Propagation and Scattering in the Heterogeneous Earth. Springer-Vertag, Berlin, pp. 308.